THE ASTRONOMICAL JOURNAL, 119:2341–2348, 2000 May
© 2000. The American Astronomical Society. All rights reserved. Printed in U.S.A.

THE SPECTRUM OF TMR-1C IS CONSISTENT WITH A BACKGROUND STAR

S. TEREBEY,[1] D. VAN BUREN,[2] K. MATTHEWS,[3] AND D. L. PADGETT[2]

Received 1999 August 23; accepted 2000 January 25

ABSTRACT

In a previous paper we proposed that there may be a population of runaway planets and brown dwarfs that formed via ejection from multiple-star systems. We further suggested TMR-1C as a candidate runaway protoplanet. *Hubble Space Telescope* NICMOS images of the Class I protostar TMR-1 (IRAS 04361+2547) reveal TMR-1C as a faint near-infrared companion with $10''.0 = 1400$ AU projected separation. The central protostar is itself resolved as a close binary with $0''.31 = 42$ AU separation, surrounded by circumstellar reflection nebulosity. A long, narrow filament seems to connect the protobinary to the faint companion TMR-1C, suggesting a physical association, which can plausibly be explained if TMR-1C was ejected by the protobinary. This paper presents near-infrared grism spectroscopy to constrain the effective temperature of TMR-1C, obtained with the Near-Infrared Camera (NIRC) at Keck Observatory. To interpret the data, we construct a grid of extincted M dwarf spectra to compare with the low-resolution ($R \sim 120$) NIRC spectrum. The assumed extinction corresponds to standard interstellar dust. With the additional assumption that no near-infrared dust excess contributes to the spectrum, then M4.5 is the latest spectral type TMR-1C can have within the uncertainties. Adopting 2 σ error bars, this translates to $T_{\rm eff} > 2700$ K effective temperature and $A_K = 2.5 \pm 0.75$ extinction at K band ($A_V = 22 \pm 6.6$ for standard dust). We compare the luminosity and effective temperature of TMR-1C with evolutionary tracks of young giant planets and brown dwarfs in a theoretical H-R diagram. Given a relatively low inferred luminosity of $\sim 10^{-3}\ L_\odot$, then TMR-1C is hotter than predicted by available theoretical models. However, the models are very uncertain at such young ages, less than 300,000 yr, so that it is unclear whether the theoretical tracks by themselves provide a suitably strong test. Given the quality of the observed spectrum, only a partial answer is possible. The new data do not lend weight to the protoplanet interpretation, and the results remain consistent with the explanation that TMR-1C may be a background star. We discuss additional observational tests that may be useful.

Key words: binaries: general — circumstellar matter — infrared radiation — planetary systems — stars: formation — stars: individual (TMR 1)

1. INTRODUCTION

The number of detected extrasolar giant planets around nearby stars continues to increase rapidly, nearing two dozen at last count (Marcy & Butler 1998; Marcy, Cochran, & Mayor 2000). The relatively close proximity of faint planet to bright star (~ 3 AU) in recent radial velocity searches makes direct detection of extrasolar planets a daunting technical challenge. In a recent paper we suggested that *isolated* planets and brown dwarfs could arise via ejection from a parent binary star system, leading to "runaway" substellar objects (Terebey et al. 1998). The importance of isolated substellar objects is that they can be studied by direct imaging and spectroscopy using current technology.

The suggestion that substellar objects may be ejected from multiple stellar systems has a firm theoretical basis. Classical studies of few-body systems in celestial dynamics find that, apart from some exceptions, such as hierarchical systems, three-body stellar systems with comparable separations are unstable and tend to eject the lowest mass object (Standish 1972; Monaghan 1976). Sterzik & Durisen (1998) revisit and confirm this result in the modern context of multiple star formation. They find that few-body systems ($N = 3$, 4, or 5) with no dissipation decay to mostly single star or binary outcomes. Moreover, the single stars, which in this study are necessarily ejected, have the lowest masses and highest velocities. This mechanism applies to stars, but it applies equally well to lower mass objects such as brown dwarfs, which might be thought to satisfy the assumption of a spherical rather than flattened initial N-body distribution.

In the case of planets, planet formation likely takes place in a disk. A relevant study is that of Levison, Lissauer, & Duncan (1998), who investigate the stability of solar systems in the context of classical planet formation theory. Starting with a swarm of Earth-mass planet embryos in a gaseous disk, they find somewhat unexpectedly that planetary bodies are often ejected, swallowed by the star, or migrate outwards. Their simulation requires very high levels of eccentricity-damping dissipation even to match the highly eccentric orbits of observed extrasolar planets. Further work needs to be done, but if these two studies capture the essential physics, then there may be reason to expect a substantial population of runaway planets and brown dwarfs.

The difference between brown dwarfs and giant planets remains a matter of active debate; we purposefully make no distinction between them. Brown dwarf searches are increasingly successful in finding likely brown dwarfs in a variety of evolutionary states ranging from old field brown dwarfs, intermediate age (10^7–10^8 yr) brown dwarfs in stellar clusters, and young brown dwarfs (10^6–10^7 yr) in star-forming regions (Nakajima et al. 1995; Basri, Marcy, & Graham 1996; Rebolo et al. 1996; Luhman, Liebert, & Rieke 1997; Briceño et al. 1998; Neuhäuser & Comerón

[1] Extrasolar Research Corporation, 569 South Marengo Avenue, Pasadena, CA 91101.
[2] Jet Propulsion Laboratory, IPAC 100-22, California Institute of Technology, Pasadena, CA 91125.
[3] Department of Physics, Mail Stop 320-47, California Institute of Technology, Pasadena, CA 91125.

1998; Rebolo et al. 1998; Wilking, Greene, & Meyer 1999; Itoh, Tamura, & Nakajima 1999). The inferred masses of isolated brown dwarfs are highly model dependent; uncertainties in age, temperature, and theoretical tracks currently limit the accuracy of derived masses. A recent study uses the GG Tau quadruple system to test different theoretical tracks by assuming coeval formation of the four young stars; the authors further conclude the faintest member is a young brown dwarf (White et al. 1999).

Theoretical models predict that giant planets and brown dwarfs are hottest and brightest when young (D'Antona & Mazzitelli 1994, 1997; Burrows et al. 1997; Baraffe et al. 1998), thus motivating searches for young brown dwarfs in star-forming regions and star clusters. In the nearby ρ Oph molecular cloud, several studies identify candidate young brown dwarfs, a number of which also exhibit near-infrared excesses (Wilking et al. 1999; Comerón et al. 1998). The near-infrared excess is evidence for hot dust near the young brown dwarf candidates, in direct analogy to young stellar objects (YSOs) and protostars, which commonly exhibit near-infrared excesses due to dusty circumstellar disks.

We have proposed that TMR-1C, a faint near-infrared object detected near the Class I protostar TMR-1 using *Hubble Space Telescope* (*HST*) NICMOS, may be a runaway protoplanet (Terebey et al. 1998). If TMR-1C has the same distance as the protostars (140 pc), and is the same age ($\sim$100,000–300,000 yr) or younger, then its flux is consistent with models of giant planets and brown dwarfs. Models further predict an effective temperature that corresponds to M or L spectral types. Previous *HST* NICMOS photometry was not sufficient to establish effective temperature. Dust extinction and effective temperature are highly coupled; the analysis was further complicated by the nonstandard *HST* NICMOS filters, preliminary flux calibration (10%), and the possibility that TMR-1C might have a near-infrared dust excess. In this paper we present near-infrared spectroscopy of TMR-1C to constrain the object's effective temperature. In principle, $R \sim 100$ resolution is sensitive to broadband water features, which dominate the near-infrared spectrum of M spectral types. Higher resolution $R \sim 300$, sufficient to detect photospheric lines, would have been desirable, but with $K = 17.9$ mag TMR-1C was beyond the reach of instruments available in 1998.

2. OBSERVATIONS, DATA REDUCTION, AND CALIBRATION

We used the Near Infrared Camera (NIRC; Matthews & Soifer 1994) on the Keck I Telescope to obtain low-resolution spectra of TMR-1 using the grism mode with the *HK* filter, a filter (1.5–2.4 μm) that encompasses the standard *H* and *K* filter passbands. Table 1 summarizes relevant observing parameters from two half-nights of observing at Keck. NIRC has a 256 × 256 InSb array with 0.″15 pixels and 38.″4 field of view (FOV). Few suitable guide stars were available in this dark cloud region; we found one at P.A. = 75° (position angle east of north). The NIRC detector and slit are oriented perpendicular to this direction, so that the observed frames have P.A. = 165°.

Figure 1 shows a NIRC *K* image of the TMR-1 field. There is extensive nebulosity, which is primarily due to scattered light from the central protostars. The relation of the filament to the molecular outflow is discussed in Terebey et al. (1998). In this figure only, the image is rotated by 180° to provide a more standard image orientation. The slit (top and bottom marked) is a vertical column 4.5 pixels (0.″675) wide that passes over the pointlike target TMR-1C. By happenstance the slit traverses the bright filament above, and it falls very near (4 pixels distance) the central stars of the TMR-1 protobinary. Fortunately there is little nebulosity below the target TMR-1C, which facilitated subsequent subtraction of OH night-sky lines. Several faint objects are seen in the Keck NIRC image (38″ FOV), all of which fall outside the previous *HST* NICMOS 19″ field of view. The object somewhat fainter than TMR-1C, located about 6″ below and to the left, is extended, thus suggesting that it may be an H_2 emission knot. The two next brightest objects, at $K = 19.7$ and 19.9, are 1.8–2.0 mag fainter than TMR-1C, with sizes that are only marginally larger than the point-spread function (PSF), so that they could be unrelated field stars.

The observed number of faint objects in the NIRC image (Fig. 1) is consistent with previous background star estimates, when updated for the extinction derived in § 4.1 (Terebey et al. 1998). For the Taurus cloud, the unextincted *K*-band star count is about $N(K' < K) = 0.065 \times 10^{0.32K}$ stars deg^{-2} (Beichman & Jarrett 1994). Adopting $A_K = 2.5$ across the 38.″4 NIRC FOV, the predicted number of sources brighter than $K = 20$ is 2.9, which agrees well with the possible background sources at this magnitude limit given small number statistics. We forego computing the chance of TMR-1C's near proximity to the filament given that it requires a posteriori statistics, which is always a difficult issue.

The extensive nebulosity precluded standard on-chip sky-background chopping. Therefore we alternated target and off-chip sky frames (−40″ nod in *y*-direction). The

TABLE 1

OBSERVING LOG WITH NIRC ON KECK I

Date	Name	Filter	Mode	T_{int} (s)	N[a]	Air Mass	SS Air Mass[b]
1998 Sep 27.....	TMR-1	*K*	Image[c]	300	5	1.32–1.00	
		HK	Grism	1040	7	1.25–1.10	1.18[d]
		HK	Grism	1280	7	1.01–1.03[e]	1.03
1998 Sep 28.....	BRI 0021−0214	*HK*	Grism	24	2	1.18	1.01

[a] Number of frames co-added.

[b] Air mass of spectral standard. The spectral standard used, HD 285801 G1 V (Castelaz et al. 1991), was observed immediately before or after the target.

[c] Protostar peak saturated to maximize exposure time on fainter TMR-1C.

[d] The standard spectrum used was constructed from the geometric mean of two spectra with air masses of 1.35 and 1.03, respectively.

[e] Target observed before and after transit.

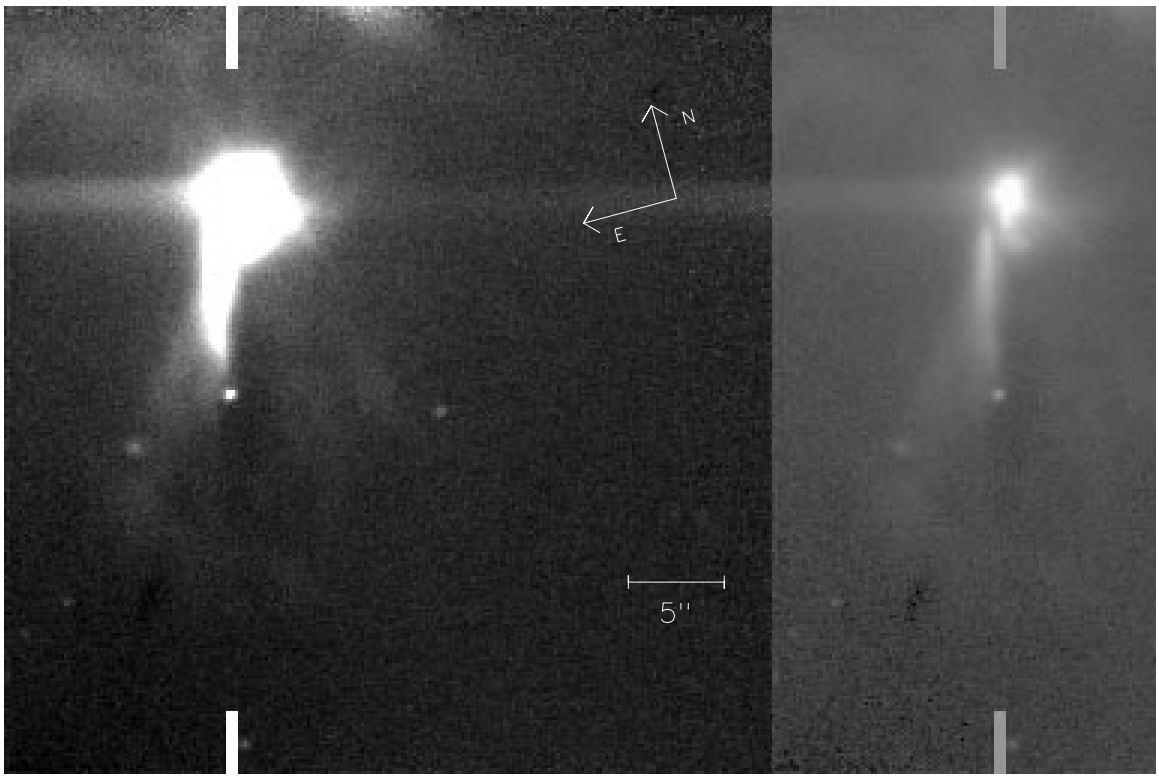

FIG. 1.—A Keck K (2.2 μm) image of the protobinary TMR-1 showing extensive nebulosity over the 38.″4 field of view. A narrow filament extends 10″ = 140 AU from the protobinary to TMR-1C, the faint candidate protoplanet. The position and approximate width of the NIRC grism slit are marked. In this figure only, the image is rotated by 180° to provide a more standard image orientation. Left frame shows linear stretch. Right frame shows logarithmic stretch.

target was observed at three positions along the slit, 0, ±1″, to minimize bad-pixel problems. The skies were mostly clear but not photometric, with very good (2.5 pixels = 0.″38) and at times excellent seeing.

There was no standard reduction package available, so data reduction procedures were written in IDL. Given the strong interest in these observations, we describe the reduction in greater than usual detail. First, target–sky frame pairs were subtracted, then deglitched using median replacement of outliers in a 3 × 3 pixel box. The not quite vertical (6 pixel variation) slit profile was rectified to be vertical, removing the horizontal offset on a row-by-row basis. The images were then flattened, dividing by an HK + grism–generated dome flat to take out vertical (constant wavelength) sensitivity variations.

There were vertical offsets between frames due to the ±1″ dithering. The frames were registered vertically, accurate to 0.1 pixels. In addition, the spectra were not perfectly horizontal. There was a 3 pixel droop, which we approximated using a parabolic fit to the ridgeline of the spectral standard star. This vertical droop was rectified column by column, accurate to 0.1 pixels. The final local background subtraction removed residual OH night-sky lines by subtracting the average of 20 rows directly above the target. The images were divided by integration time to give instrumental units of DN s^{-1}. Frames were weighted by integration time to produce the final co-added image.

The reduced grism images for TMR-1 plus standard stars are available as FITS files in the electronic edition of the Journal. Figure 2 shows the co-added reduced grism image of the TMR-1 field, with P.A. = 165° (which differs from the Fig. 1 orientation by 180°). The slit/spatial direction is vertical, while the wavelength direction is horizontal. The broad vertical band midchip is due to telluric water absorption near 1.9 μm. The target TMR-1C is a horizontal band–

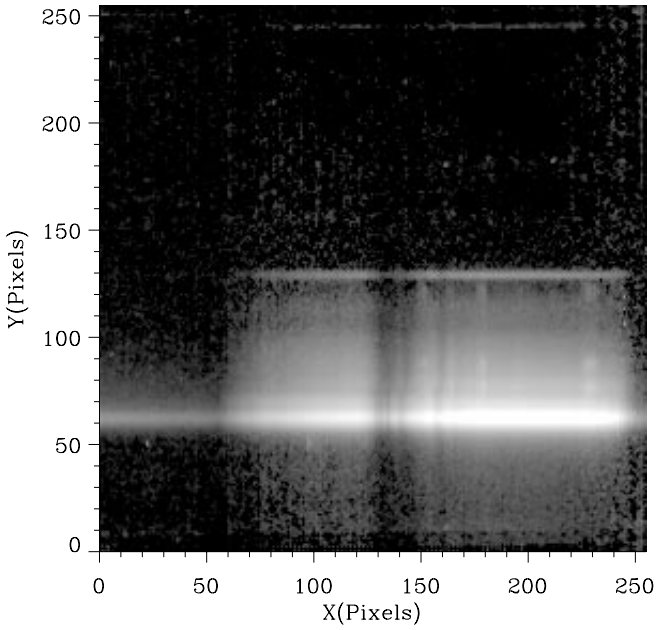

FIG. 2.—The reduced Keck NIRC grism image of the TMR-1 field. The slit/spatial direction is vertical, while the wavelength direction is horizontal. The candidate protoplanet appears at row 129, the protobinary near row 64, with filament emission between.

TABLE 2

COMPUTED $H-K$ COLORS USING GRISM SPECTRUM

Name	$H-K$ (Observed)	$H-K$ (Recovered)[a]
Melotte 22 MSK 18 G8 V.....	0.07[b]	0.07
BRI 0021−0214	0.54[c]	0.53
TMR-1C	1.75[d]	1.46

[a] The $H-K$ color reconstructed from the NIRC grism spectrum.

[b] Quoted color is based on spectral type. Values adopted were $H-K$ colors of 0.05 for G1 V and 0.07 for G8 V, from Tokunaga 2000. This test measures the (small) color difference between our G1 V and G8 V standard stars.

[c] Photometry of this star is $J = 11.83$, $H = 11.09$, $K = 10.55$ (Persson et al. 1998).

[d] Blake et al. 2000.

centered midchip at row 129. Below is seen mostly continuum emission from the bright filament. The brightest row, row 64, is where the slit passes closest to the central TMR-1AB protobinary. The slight offset to the left arises because the left edge of the slit is most highly illuminated by the slightly offset protostars. Here and elsewhere we show the second of our TMR-1 observations listed in Table 1 because of its better quality (air mass, integration time, seeing). The first data set gives consistent results but has somewhat lower signal-to-noise ratio.

A spectrum is "extracted" from the image and then divided by a star of known spectral type, the spectral standard, to correct for instrumental efficiency and telluric absorption. Over the $H-K$ bandpass G dwarfs have weak spectral features, the strongest being Brγ at 2.166 μm. The primary spectral standard selected was the G1 V star HD 285801, observed close in time and close in air mass to the target (see Table 1). A second spectral standard (see Table 2), a G8 V dwarf, was observed to check consistency. The ratio of the two standard-star spectra versus wavelength was nearly flat, as desired. The ratio of G1 to G8 star showed a smooth variation with wavelength at the 10% level, which we take as a measure of the large-scale reliability of the spectral slope extraction over the filter passband.

The extensive nebulosity in Figure 2 complicates the spectral extraction and favors a narrow extraction window. But, if the seeing is wavelength dependent, a fixed extraction window can introduce spurious wavelength effects by undercounting flux. Fits to the grism standard-star data showed that the PSF decreased with wavelength, on order 20% smaller at 2.2 μm compared with 1.6 μm. Tests showed the blue/red undercounting was an acceptable 2% for the 7 pixel (1.″05) extraction window selected for TMR-1C.

Figure 3 shows the instrumental spectrum extracted for TMR-1C, before division by the spectral standard. This and subsequent spectra are Hanning smoothed with a [0.25, 0.50, 0.25] pixel kernel. The uncertainty of the mean spectrum is fairly constant versus wavelength with $\sigma = 0.37$ counts s^{-1}, estimated from the seven contributing observations. The dashed line shows the fractional uncertainty computed relative to the mean spectrum. The fractional uncertainty increases at the edges of the filter passband and in the broad 1.9 μm telluric water band. The fractional uncertainty is lowest in the red 2 μm window at about 0.04, which inverted gives roughly 25:1 per Hanning-smoothed pixel for the dynamic range.

3. NEAR-INFRARED SPECTRUM OF TMR-1C

The top spectrum in Figure 4 shows TMR-1C after dividing the spectral standard. The flux relative to the spectral standard is a convenient representation: to convert to physical units multiply by f_λ or f_ν of a G1 V star, which in the near-infrared is closely approximated by a Planck function with 5880 K effective temperature.

The spectrum of TMR-1C is roughly linear across the passband, its appearance dominated by dust extinction. There are residual atmospheric H_2O features in the 1.8–2.0 μm region. Possible absorption features near 2.3 μm are

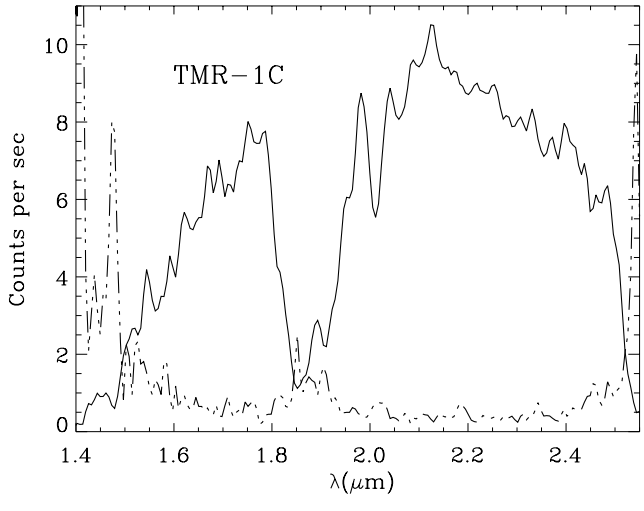

FIG. 3.—Extracted TMR-1C spectrum, Hanning smoothed, before division by spectral standard (*solid line*), showing broad telluric H_2O absorption near 1.9 μm, as well as the edges of HK filter bandpass. The TMR-1C mean spectrum has a standard of deviation σ of 0.37 counts s^{-1}, estimated from the seven contributing frames. The dot-dashed line shows the fractional noise times 10, with fractional noise defined as σ divided by the spectrum. The noise is low and well behaved near 2.3 μm, with a value of 0.04, which inverted gives 25:1 for the dynamic range.

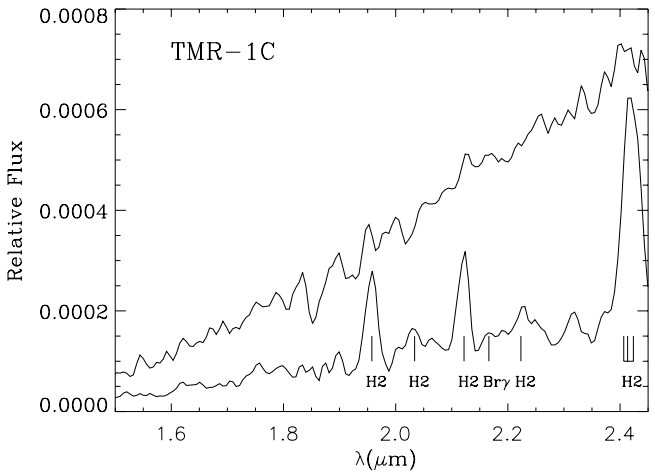

FIG. 4.—NIRC spectrum of TMR-1C plus nearby emission knot in the filament. The top spectrum shows TMR-1C after division by the spectral standard. The appearance of the spectrum is dominated by dust extinction. Residual telluric H_2O and higher noise are apparent in the 1.8–2.0 μm spectral region. Lower spectrum shows a nearby $\sim 1''$ H_2 emission knot in the filament, multiplied by 0.8 for clarity. The estimated contribution of the filament to TMR-1C's spectrum is less than 10%.

discussed in § 4.1. The dynamic range is about 25:1 per pixel in the 2 μm region. There is also an estimated uncertainty of 15% in the spectral slope (§ 4.1).

The lower spectrum in Figure 4 shows a nearby bright emission knot in the filament, located 8 pixels below (i.e., 1".2 north). The spectrum exhibits three H_2 emission-line features, a common shock by-product near YSOs, which by happenstance permit us to check the wavelength calibration. The nominal wavelength scale of 0.05916 μm pixel^{-1} appears adequate. Although H_2 emission lines were detected in several places along the filament, most of the filament emission is continuum, consistent with polarimetry, which implies that the filament is illuminated by scattered stellar light (Lucas & Roche 1997).

Higher spatial resolution *HST* NICMOS images (not shown) show that TMR-1C is spatially unresolved and sits 0".5 from the sharp edge of the filament (Terebey et al. 1998). As a result of the lower spatial resolution of the current data, there may be some flux contributed by the filament. By doing polynomial fits in the spatial y-direction, we estimate the filament contribution to the TMR-1C spectrum is less than 10%; subtracting it does not affect our conclusions.

4. COMPARISON WITH EXTINCTED M STAR SPECTRA

Models of *young* giant planets and brown dwarfs predict temperatures up to approximately 3000 K (e.g., Burrows et al. 1997); to first order, spectra should appear similar to M4–M5 or later spectral types. To constrain the effective temperature we compared the spectrum of TMR-1C with those of extincted M stars. The comparison M star spectra are from Wilking et al. (1999, hereafter WGM).

A late-type M star in Figure 5 illustrates the characteristic features of M spectral types at near-infrared wavelengths (see also WGM). The CO photospheric absorption lines near 2.3 μm are prominent for all classes; Na and Ca are also seen. For M6 and later, the CO band head at 2.28 μm becomes very prominent. For M2 and later, a broad H_2O absorption feature appears near 1.9 μm and becomes progressively deeper at later spectral classes.

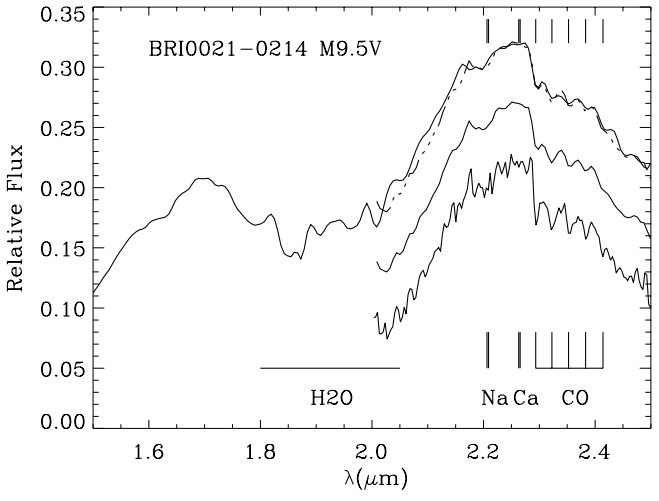

FIG. 5.—Comparison of NIRC M9.5 V spectrum with WGM spectrum for the same object, BRI 0021−0214, showing excellent agreement. Bottom spectrum is the WGM spectrum. Middle spectrum shows WGM after resampling and smoothing to the NIRC resolution, repeated as a dashed line overlaid on the NIRC (*top*) spectrum. There is a broad H_2O absorption feature from 1.8 to 2.0 μm. Photospheric CO lines are also seen near 2.3 μm. Lower two spectra are offset by a constant for clarity, −0.05 and −0.10, respectively.

Figure 5 shows a comparison of our NIRC grism spectrum with the WGM spectrum for the same object, BRI 0021−0214, a very cold object classified as >M9.5 that has approximately 2200 K effective temperature (Kirkpatrick, Henry, & Simons 1995). The top spectrum is our NIRC grism spectrum, which clearly demonstrates that NIRC has sufficient spectral resolution to detect the photospheric CO absorption lines. The NIRC spectrum is divided by the G1 V spectral standard and has an estimated $R \sim 120$ spectral resolution. The bottom spectrum shows the WGM spectrum, which has higher spectral resolution ($R \sim 300$) but covers a smaller wavelength range. The middle spectrum shows the process of matching the WGM spectrum to a NIRC spectrum by smoothing to lower spectral resolution, converting from an A0 to G1 spectral standard, and resampling to the NIRC pixel spacing. There is excellent agreement between our NIRC grism spectrum and the WGM matched spectrum (overlaid as dashed line); the only two adjustable parameters are an arbitrary multiplicative constant related to the absolute flux scale, plus the amount of spectral smoothing.

4.1. *With Dust Extinction*

The near-infrared spectra of young objects in star-forming regions are dominated by dust extinction (e.g., Greene & Lada 1996). At near-infrared wavelengths dust extinction shows much less variation than at visible wavelengths, so that the dust extinction law is well represented by a power law whose absolute value is approximately independent of line of sight (Cardelli, Clayton, & Mathis 1989; Martin & Whittet 1990; Mathis 1990). We adopt an empirically based extinction law (B. Draine 1999, private communication) that has $A_\lambda \sim \lambda^{-1.6}$ and also adopt $A_K = 1.73E(H-K)$. The values quoted in the literature vary by 10% for both numbers so that we estimate the uncertainty in the extinction determination is at least 15% and possibly greater.

We compared our spectrum of TMR-1C with extincted stellar spectra ranging from K5 V to M9.5 V spectral type. Figure 6 shows the latest spectral type, M4.5, which is consistent with our data. Later spectral types show too much spectral curvature due to the progressively deeper H_2O band.

This conclusion depends on the level of uncertainty in the NIRC spectrum, particularly those due to systematic effects. The spectrum is constructed by extracting the source data and dividing by the extracted standard-star data. Various effects produce systematic errors that lead to large-scale undulations, namely, curvature in the spectrum; one example is seeing, which for these data is both wavelength dependent and time variable. We estimated the extraction reliability with high signal-to-noise data to be 10% using the available standard-star frames (§ 2). The spectrum of TMR-1C also contains contamination from the filament at the 10% level; adding the uncertainties in quadrature seems reasonable and leads to an estimated 15% 1 σ uncertainty due to systematic effects. As a further test of the reliability of the TMR-1C spectrum we computed synthetic $H-K$ colors. Briefly, we converted spectra to f_λ and computed H and K instrumental magnitudes by transforming between the known filter passbands. The results, shown in Table 2,

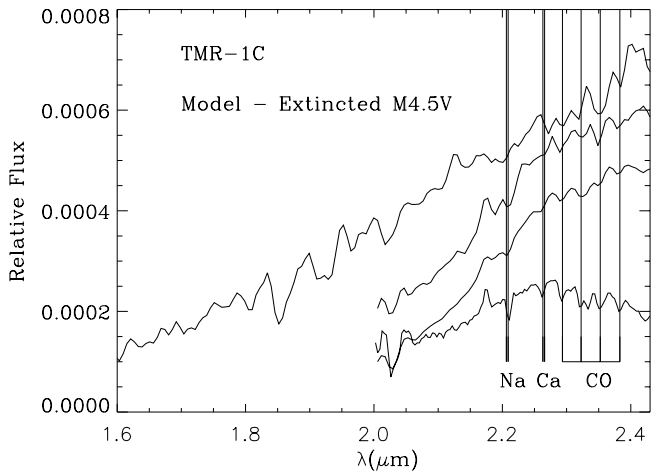

FIG. 6.—Comparison of TMR-1C spectrum with an extincted M star. We conclude M4.5 is the latest spectral type consistent with the data. The spectrum may show evidence of CO lines, which would suggest the spectral type is not earlier than K5. Bottom shows WGM M4.5 V spectrum. Next higher shows *extincted* WGM spectrum resampled to NIRC resolution. Spectrum above has noise added, corresponding to that measured for the NIRC data. Middle two spectra are offset for clarity by a constant, −0.0001 and −0.0002, respectively.

show good correspondence except for our faint red object, TMR-1C. The difference of 0.3 mag between the synthetic and observed $H-K$ colors corresponds to 2 σ, not a significant difference. However, note that this term represents a systematic uncertainty that affects the overall spectral slope, the sense of which is that TMR-1C's spectrum may be up to 30% steeper than shown by the NIRC data.

Our constraint on spectral type was made using fits to M standard stars over a restricted wavelength range covering the K-band window. We now consider whether a larger spectral window spanning the broad 1.9 μm water feature would improve the constraint and conclude that further improvements are unlikely given the low spatial frequency component of the uncertainty. Consider the extincted M4.5 spectrum in Figure 6. The water feature is visible as curvature in the spectrum shortward of about 2.2 μm. A spectrum with wider spectral coverage would show the water feature extending to roughly 1.7 μm with a relative minimum at 1.9 μm. We estimate the magnitude of the 1.9 μm dip to be 28% below a linear fit to the relative flux between 1.6 and 2.2 μm, derived from M4 data in Leggett et al. (1996). This suggests that wider spectral coverage would show the broad water feature deviates from linearity by about 2 σ, which is not significant given the predominantly systematic uncertainties. Out of concern that a tighter constraint would overinterpret the observations we conclude that M4.5 is the latest spectral type consistent with the observed spectrum.

In general, extinction and effective temperature are degenerate, so that the spectral type cannot be further constrained unless spectral features are visible. The observed spectrum of TMR-1C shows features that may indicate CO lines in the 2.3–2.4 μm range. This range fortunately falls in a low-noise and well-behaved part of the NIRC spectrum. The bottom spectrum in Figure 6 is an unextincted M4.5 standard from WGM. The next higher spectrum is smoothed and resampled to the NIRC spectral resolution. Also applied is the nominal dust extinction $\tau = 2.3$ at 2.2 μm implied by the $H-K = 1.46$ color excess, using $\tau = A_\lambda/1.086$ and assuming intrinsic $(H-K)_0 = 0.29$ for M4.5 V spectral type. The spectrum above shows the effects of adding noise, where the noise is the noise per pixel estimated from the TMR-1C data (shown in Fig. 3), but does not include the uncertainty in spectral slope and shape. The displayed model spectrum with noise represents one of many possible realizations; from viewing many such spectra we observe that noise at this level tends to wipe out one of the four CO lines. In addition, we performed a χ^2 test, fitting a restricted region near the CO lines with M star spectra that in one case had normal CO lines and in the other case had the CO lines smoothed away. Including the CO lines significantly improved the reduced χ^2 of the fit. However, the case that had no CO lines cannot be ruled out with these data, for which the reduced χ^2 value corresponds to a 2 σ result. Therefore these data provide suggestive but not conclusive evidence for CO absorption lines. If CO lines are present this constrains the spectral type to be later than approximately K5 V spectral type.

We now compute the absolute K magnitude for M4.5 V spectral type, which is a limiting case. The apparent magnitude $K = 17.88 \pm 0.1$ (Blake, Koresko, & Brown 2000) and DM $= 5.7 \pm 0.2$ distance modulus (140 pc) for a source that lies within the Taurus cloud. From the previous paragraph the derived dust extinction is $A_K = 2.52 \pm 0.38$ (15% uncertainty). This implies $M_K = 9.6 \pm 0.8$ (2 σ) absolute magnitude. Earlier spectral types have a modestly (up to 10%) larger extinction correction, so, for example, M_K decreases to 9.2 for K5 spectral type. Larger distances, such as appropriate for a background source, imply intrinsically higher flux.

5. BACKGROUND STAR HYPOTHESIS

We have suggested that TMR-1C is a young substellar object; the alternate explanation is TMR-1C is a background star that is unrelated to the observed near-infrared filament. Here we describe the likely properties of a background object. First, TMR-1C has Galactic coordinates (174°, −14°), showing that it lies in direction of the Galactic anticenter, therefore minimizing the background source counts. Galactic structure models show that for $K > 16$ the K-band source counts are dominated by disk dwarfs (Beichman & Jarrett 1994). We set a fiducial maximum distance of 2.5 kpc, which corresponds to a star that lies 1 scale height off the Galactic plane, where 600 pc is adopted for the old disk scale height. Correcting for extinction, the K magnitude is consistent with M, K, and G dwarf stars behind the Taurus cloud, out to 2.5 kpc distance.

6. COMPARISON WITH YOUNG GIANT PLANET AND BROWN DWARF MODELS

For the hypothesis that TMR-1C is a young substellar object, the age of TMR-1C ranges from the (2–3) × 10^5 yr lifetime of the parent protostars, to as young as the ∼2000 yr age of the filament. This age is much shorter than the 1–10 Myr required by the standard model of gas-giant planet formation (Pollack et al. 1996). Formation of substellar objects during the protostar phase might occur in several ways. It may be a natural by-product of star formation, in a picture where "seed" masses form, grow, and interact to eventually form a binary system (Bonnell & Bate 1994; Bate 1997). Gas giant planet formation by disk instability is an alternate mechanism which leads to rapid planet

formation (Boss 1997, 1998). A third possibility is gravitational instability in the filament itself (Lin et al. 1998). A consequence of the young age is that quantitative comparison with available models for young planet and brown dwarfs is problematic, as below 1 million years age the models are sensitive to initial conditions since the thermal relaxation timescale is comparable to the planet's age. To make the comparison also requires translating observational parameters into luminosity and effective temperature, steps that introduce substantial uncertainty.

We adopt the WGM temperature scale, which covers the full range of M spectral types. It is similar to that of Leggett et al. (1996), who in addition cite ± 150 K for the uncertainty. This gives an effective temperature of 3000 ± 300 K ($2\ \sigma$) for an M4.5 V star, which implies that 2700 K is the lowest effective temperature consistent with the NIRC data. To estimate the bolometric luminosity we fit the observed near-infrared photometry using a blackbody spectrum extincted by dust. We express the extinction in A_V rather than A_K [using $A_V = 15.4E(H-K)$] for ease of comparison with previous results. For a distance of 140 pc, assuming TMR-1C is in the Taurus cloud then the bolometric luminosity is approximately $1 \times 10^{-3}\ L_\odot$, ranging from 5×10^{-4} to 3×10^{-3} for $T_{\rm eff} = 3000$ K and $A_K = 2.5 \pm 0.75, 2\ \sigma$ ($A_V = 22 \pm 6.6$). The derived extinction is higher than our previous estimate, leading to luminosities that are roughly a factor of 3 higher (Terebey et al. 1998).

Figure 7 shows a theoretical H-R diagram, on which are plotted the 1998 D'Antona & Mazzitelli stellar and brown dwarf evolutionary tracks (D'Antona & Mazzitelli 1994, 1997). Different input physics leads to systematic differences between the available models (D'Antona & Mazzitelli 1994, 1997; Burrows et al. 1997; Baraffe et al. 1998). The rectangular box displays the $2\ \sigma$ error box for TMR-1C at the Taurus cloud distance, where it is seen that the allowed region straddles the substellar boundary of approximately $0.08\ M_\odot$. Given the derived luminosity and proposed young age of TMR-1C, the models suggest a temperature that is substantially colder than that demonstrated by the data.

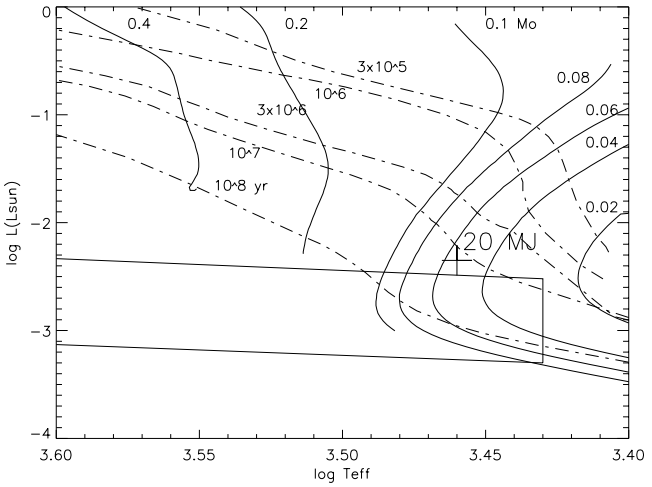

FIG. 7.—Theoretical H-R diagram with $2\ \sigma$ error box (*solid line*) shown for TMR-1C. Theoretical evolutionary tracks are plotted for different masses (solid lines labeled in $M_\odot$) and ages (*dot-dashed lines*) for the models of D'Antona & Mazzitelli (1994, 1997). The stellar-substellar boundary falls near 0.07–0.08 $M_\odot$. The track locations should be considered indicative as there are significant differences between theoretical models (D'Antona & Mazzitelli 1994, 1997; Burrows et al. 1997; Baraffe et al. 1998). The predicted temperatures of giant planets are cooler than seen for TMR-1C. However, appropriate models for TMR-1C that incorporate accretion luminosity are not yet available and may shift the tracks considerably. This is illustrated by the point labeled 20 M_J, which shows the model for TMR-1C proposed by Lin et al. (1998) for a 2500 yr object that formed out of filament material.

7. DISCUSSION

We return to the question of whether the assumptions used in young giant planet and brown dwarf models are appropriate for the case of TMR-1C. A simple calculation suggests the accretion history of young substellar objects cannot be ignored for ages less than 1 million years. Suppose a giant planet is formed with constant accretion rate, for example, $10M_J$ in 3×10^5 yr. Then the accretion luminosity during formation is $L_{\rm acc} \sim G\dot{M}M/R$, where G is the gravitational constant, M is the object's mass, $\dot{M}$ is the accretion rate, and R is the object's radius. For the typical $R = 2.0$, $R_J \sim 0.2\ R_\odot$, then $L_{\rm acc} = 0.05\ L_\odot$. This accretion luminosity is roughly 30 times higher than the $10M_J$ model at similar age of Burrows et al. (1997). The estimated accretion luminosity is $0.005\ L_\odot$ for $3M_J$, about 15 times higher than nonaccreting models. The importance of accretion luminosity is well established in the case of protostars, where theoretical calculations show it acts to increase both the star's luminosity and effective temperature (Stahler, Shu, & Taam 1980a, 1980b, 1981).

If TMR-1C was formed near the protostars and recently ejected, then accretion would have stopped abruptly several thousand years ago, implying the surface temperature and luminosity could still be elevated and resemble those of an accreting object. Quantitative numbers await the availability of models that include accretion; until then the model of Lin et al. (1998) illustrates the temperatures and luminosities that may be achieved. In their model they propose TMR-1C may have formed from a tidal tail created by the disruption of a circumstellar disk, so that the age of the object matches the age of the filament out of which it formed. They suggest parameters with $T_{\rm eff} = 2900$ K and $0.004\ L_\odot$ for an age of 2500 yr for an $M = 20M_J$ object. This model point is plotted in Figure 7, where it appears very close to the TMR-1C error box. This illustrates that a better theoretical understanding of how substellar objects evolve during their earliest phases is needed before tests using theoretical H-R diagrams can be made with confidence. Moreover, the lack of applicable models makes it difficult to even know how to recognize a young ejected substellar object.

The quality of the observed spectrum is not high enough to determine what TMR-1C is. However, the results of the new experiment do not lend additional weight to the idea that TMR-1C is a runaway planet. Instead the results are ambiguous but not encouraging, and they remain fully consistent with the possibility that TMR-1C is a background low-luminosity star. A more definitive answer may come from observational tests with greater power to distinguish whether TMR-1C is an ejected protoplanet or a normal background star. The proper motion predicted for an ejected object moving at 2–5 km s^{-1} should be detectable in several years, for example, with a refurbished NICMOS camera on *HST*. Broadband photometric monitoring may show variability similar to YSO variability associated with changes in circumstellar material. Also, the presence or

absence of a near-infrared dust excess, which distinguishes between a young and old object, is testable with high-precision (<0.1 mag) broadband photometry. Finally, young objects have larger radii and thus lower surface gravity than evolved objects, so that spectral lines should show subdwarf characteristics (e.g., Luhman et al. 1997). Higher resolution $R \sim 300$ spectroscopy will be capable of detecting photospheric lines with sufficient signal-to-noise ratio for a $K = 18$ object, using the new generation of near-infrared instruments on large telescopes.

We thank Gary Chanan for his generosity at Keck and thank the Keck staff, including R. Goodrich, for excellent observing support. We also thank Lee Armus, Peter Bodenheimer, Alan Boss, Andi Burkert, Adam Burrows, Greg Laughlin, Gerry Neugebauer, and Frank Shu for useful discussions. S. T. gratefully acknowledges NASA support, including funding through the Origins of Solar Systems Program under contract NAS W-97009, and funding from grant GO-07325.01-96A through the Space Telescope Science Institute, which is operated by the Association of Universities for Research in Astronomy, Inc., under NASA contract NAS 5-26555. This work was carried out in part at the Jet Propulsion Laboratory, operated by the California Institute of Technology under contract for NASA. Data presented herein were obtained at the W. M. Keck Observatory, which is operated as a scientific partnership among Caltech, the University of California, and NASA. The observatory was made possible by the generous financial support of the W. M. Keck Foundation.

REFERENCES

Baraffe, I., Chabrier, G., Allard, F., & Hauschildt, P. H. 1998, A&A, 337, 403
Basri, G., Marcy, G. W., & Graham, J. R. 1996, ApJ, 458, 600
Bate, M. R. 1997, MNRAS, 285, 16
Beichman, C. A., & Jarrett, T. 1994, Ap&SS, 217, 207
Blake, G., Koresko, C., & Brown, M. 2000, in preparation
Bonnell, I. A., & Bate, M. R. 1994, MNRAS, 271, 999
Boss, A. P. 1997, Science, 276, 1836
———. 1998, ApJ, 503, 923
Briceño, C., Hartmann, L., Stauffer, J., & Martín, E. 1998, AJ, 115, 2074
Burrows, A., et al. 1997, ApJ, 491, 856
Cardelli, J. A., Clayton, G. C., & Mathis, J. S. 1989, ApJ, 345, 245
Castelaz, M. W., Persinger, T., Stein, J. W., Prosser, J., & Powell, H. D. 1991, AJ, 102, 2103
Comerón, F., Rieke, G. H., Claes, P., Torra, J., & Laureijs, R. J. 1998, A&A, 335, 522
D'Antona, F., & Mazzitelli, I. 1994, ApJS, 90, 467
———. 1997, Mem. Soc. Astron. Italiana, 68, 807
Greene, T. P., & Lada, C. J. 1996, AJ, 112, 2184
Itoh, Y., Tamura, M., & Nakajima, T. 1999, AJ, 117, 1471
Kirkpatrick, J. D., Henry, T. J., & Simons, D. A. 1995, AJ, 109, 797
Leggett, S. K., Allard, F., Berriman, G., Dahn, C. C., & Hauschildt, P. H. 1996, ApJS, 104, 117
Levison, H. F., Lissauer, J. J., & Duncan, M. J. 1998, AJ, 116, 1998
Lin, D. N. C., Laughlin, G., Bodenheimer, P., & Różyczka, M. 1998, Science, 281, 2025
Lucas, P. W., & Roche, P. F. 1997, MNRAS, 286, 895
Luhman, K. L., Liebert, J., & Rieke, G. H. 1997, ApJ, 489, L165
Marcy, G. W., & Butler, R. P. 1998, ARA&A, 36, 57
Marcy, G. W., Cochran, W. D., & Mayor, M. 2000, in Protostars and Planets IV, ed. V. Mannings, A. P. Boss, & S. S. Russell (Tucson: Univ. Arizona Press), in press
Martin, P. G., & Whittet, D. C. B. 1990, ApJ, 357, 113
Mathis, J. S. 1990, ARA&A, 28, 37
Matthews, K., & Soifer, B. T. 1994, in Infrared Astronomy with Arrays: The Next Generation, ed. I. S. McLean (Dordrecht: Kluwer), 239
Monaghan, J. J. 1976, MNRAS, 176, 63
Nakajima, T., Oppenheimer, B. R., Kulkarni, S. R., Golimowski, D. A., Matthews, K., & Durrance, S. T. 1995, Nature, 378, 463
Neuhäuser, R., & Comerón, F. 1998, Science, 282, 83
Persson, S. E., Murphy, D. C., Krzeminski, W., Roth, M., & Rieke, M. J. 1998, AJ, 116, 2475
Pollack, J. B., Hubickyj, O., Bodenheimer, P., Lissauer, J. J., Podolak, M., & Greenzweig, Y. 1996, Icarus, 124, 62
Rebolo, R., Martín, E. L., Basri, G., Marcy, G. W., & Zapatero-Osorio, M. R. 1996, ApJ, 469, L53
Rebolo, R., Zapatero Osorio, M. R., Madruga, S., Béjar, V. J. S., Arribas, S., & Licandro, J. 1998, Science, 282, 1309
Stahler, S. W., Shu, F. H., & Taam, R. E. 1980a, ApJ, 241, 637
———. 1980b, ApJ, 242, 226
———. 1981, ApJ, 248, 727
Standish, E. M., Jr. 1972, A&A, 21, 185
Sterzik, M. F., & Durisen, R. H. 1998, A&A, 339, 95
Terebey, S., Van Buren, D., Padgett, D. L., Hancock, T., & Brundage, M. 1998, ApJ, 507, L71
Tokunaga, A. 2000, in Allen's Astrophysical Quantities, ed. A. Cox (New York: Springer), in press
White, R. J., Ghez, A. M., Reid, I. N., & Schultz, G. 1999, ApJ, 520, 811
Wilking, B. A., Greene, T. P., & Meyer, M. R. 1999, AJ, 117, 469 (WGM)